JOURNAL OF CATALYSIS 88, 325–332 (1984)

Decomposition of Formic Acid on Copper, Nickel, and Copper–Nickel Alloys

IV. Temperature-Programmed Decomposition of Bulk Nickel Formate and of Formic Acid Preadsorbed on Nickel Powder

E. IGLESIA AND M. BOUDART[1]

Department of Chemical Engineering, Stanford University, Stanford, California 94305

Received February 1, 1983

Formic acid (HCOOH, 6 kPa) decomposes to H_2, and surface and bulk formate upon adsorption on Ni powder at room temperature. Formate species decompose at 300–450 K to CO_2, CO, H_2, and H_2O. The CO_2 to CO ratios (3.5–5.5) are similar to those measured during decomposition of bulk Ni formate (3.5–5.0), and catalytic HCOOH decomposition on Ni powder, Ni/SiO_2, and Ni/Al_2O_3 (4.0–6.0). This suggests that the products of catalytic HCOOH decomposition on Ni arise from adsorbed formate species which decompose with a selectivity similar to that of bulk Ni formate. Structure insensitive paths seem to be preferred on fully covered surfaces.

INTRODUCTION

The temperature-programmed decomposition (TPD) of HCOOH preadsorbed at low coverage on Ni (*1–7*), Cu (*8–10*), Ag (*11*), Fe (*12*), Pt (*13*), W (*14*), and CuNi (*10*), and at high coverage on Ni single crystals (*15–17*), has been studied as a prototype of unimolecular surface reactions. On Ni, TPD selectivity and kinetics differ from those in catalytic HCOOH decomposition, apparently because the identity and surface density of adsorbed species differ in the two reactions (*18*). In contrast, similar studies on Cu suggest identical surface conditions in TPD or steady-state catalysis.

In this study, the decomposition of HCOOH preadsorbed on Ni powder is investigated at high pressure (6 kPa) and surface density ($2–6 \times 10^{15}$ cm^{-2}). The decomposition of bulk Ni formate, $Ni(OOCH)_2$, is also examined.

EXPERIMENTAL

Nickel powders designated as Ni were prepared as follows. The sample designated as Ni was obtained by precipitation of $NiCO_3$ from a nitrate solution following addition of NH_4HCO_3, heating in air at 673 K for 3 h, reduction in flowing H_2 ($\nu^b = 2.5$ h^{-1})[2] at 623 K for 24 h, and passivation. The specific surface area was 1.35 and 1.45 m^2 g^{-1} from BET and H_2 chemisorption, respectively (*19*). Another powder, designated as Ni(A), was prepared by heating $NiCO_3$ (Baker Analyzed Reagent) in flowing O_2 ($\nu^b_{O_2} = 6$ h^{-1}) at 623 K for 3 h, H_2 reduction ($\nu^b_{H_2} = 2.5$ h^{-1}) at 723 K for 24 h, and passivation. Specific surface areas were 0.55 and 0.60 m^2 g^{-1} from BET and H_2 chemisorption, respectively. The preparation and characterization of these samples was previously described (*19*).

Ni formate, $Ni(OOCH)_2$, was prepared by adding $NiCO_3$ (Baker Analyzed Reagent) to 3.5 *N* HCOOH at 323 K, $[(HCOO^-)/(Ni^{2+})] = 5$ (*20*), recrystallizing twice, and vacuum-drying at room temperature for 24 h. X-Ray diffraction (*21*) and elemental analysis showed that the product was $Ni(OOCH)_2 \cdot 2H_2O$.

[1] To whom inquiries should be addressed.

[2] ν^s_M (ν^b_M), site (s) or bulk (b) contact frequency, defined (*19*) as the number of *M* molecules entering the reactor per surface or bulk metal atom.

0021-9517/84 $3.00

Procedure

Decomposition rates and selectivity S, defined as the ratio of CO_2 to CO in decomposition products, were calculated from the concentration of products in the carrier gas, using the glass flow apparatus previously described (*22*). Concentrations of CO_2 and CO in He, and H_2 concentrations in Ar, were determined continuously by thermal conductivity measurements. Concentrations of CO_2 and CO were also measured separately at discrete intervals by gas chromatography, using a Porapak Q column and a thermal conductivity detector. In all experiments unreacted HCOOH and H_2O products were removed in a dry-ice/acetone trap before thermal conductivity measurements.

In TPD of preadsorbed HCOOH, the passivated Ni powders were first rereduced in H_2 ($\nu^s_{H_2} = 10\ s^{-1}$) at 723 K for 1 h, then flushed with He ($\nu^b_{He} = 2\ s^{-1}$) at 723 K for 0.25 h, cooled to room temperature, and exposed to HCOOH-saturated carrier gas (He or Ar, $\nu^s = 0.15\ s^{-1}$, 6 kPa HCOOH) for 300–600 s, finally flushed with pure carrier gas ($\nu^s = 2\ s^{-1}$), and heated to 723 K at a linear rate β of 0.16 K s^{-1}. Subsequent adsorption-TPD cycles were carried out without rereduction, unless otherwise noted.

A sample of $Ni(OOCH)_2 \cdot 2H_2O$ was dehydrated at 423 K in flowing He or Ar ($\nu^b = 180\ h^{-1}$) for 1.5 h before decomposition experiments. Dehydration was complete, as shown by the amount of H_2O evolved and the X-ray diffraction pattern of the residue. Isothermal and temperature-programmed decompositions were carried out in flowing He or Ar ($\nu^b = 0.02 - 2.0\ s^{-1}$).

RESULTS

TPD of Preadsorbed HCOOH

The results of TPD of HCOOH on Ni and Ni(A) powders are shown in Table 1 and Fig. 1. Dihydrogen desorbed during HCOOH adsorption at room temperature. Several desorption peaks were observed for each product during TPD. CO_2 and H_2 products desorbed simultaneously.

TABLE 1

Reaction Products and Surface Density in TPD of HCOOH Preadsorbed on Ni

	Ni	Ni(A)
CO_2 : CO	5.2 ± 0.5[a]	4.0 ± 0.5
CO_2 : H_2[b]	2.1 ± 0.2	2.2 ± 0.2
H_2 (during HCOOH adsorption) : H_2 (during HCOOH decomposition)	Not measured	0.8 ± 0.4
(CO_2 + CO) : (Ni surface atom) ("formate monolayers")	4.0 ± 0.5	4.9 ± 0.4

[a] Values are averages of two or more experiments; error reflects range of experimental values.

[b] Does not include dihydrogen desorbed during HCOOH adsorption at room temperature.

The number of Ni surface atoms was

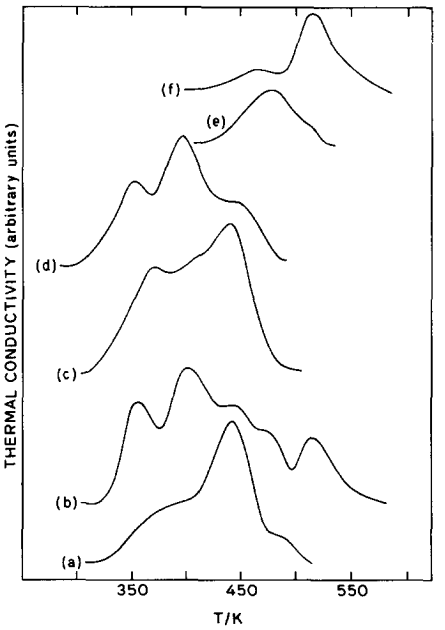

FIG. 1. Desorption of products during TPD of HCOOH preadsorbed on Ni powders. ($\beta = 0.18$ K s^{-1}, $\nu^s = 0.8\ s^{-1}$). (a) (CO + CO_2)/HCOOH (300 K), Ni; (b) (CO + CO_2)/HCOOH (300 K), Ni(A); (c) H_2/HCOOH (300 K), Ni; (d) H_2/HCOOH (300 K), Ni(A); (e) CO/HCOOH (300 K), Ni; (f) CO/HCOOH (300 K), Ni(A).

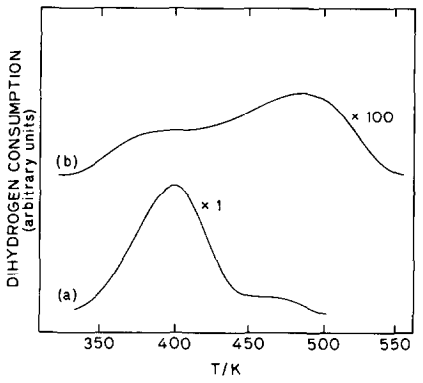

FIG. 2. Temperature-programmed reduction of Ni powder following HCOOH adsorption–decomposition experiments (reduction, $\nu^s_{H_2} = 0.4\ s^{-1}$; decomposition, $\nu^s = 0.7\ s^{-1}$; $\beta = 0.18\ K\ s^{-1}$). (a) Reduction of passivated Ni powder; (b) reduction after one HCOOH adsorption–decomposition experiment.

measured between TPD experiments by H_2 chemisorption at 20 kPa and room temperature, assuming H : Ni = 1 : 1. In HCOOH TPD, the surface density of adsorbed molecules was calculated, assuming one C per molecule, from the amount of CO_2 and CO evolved, and the number of Ni surface atoms. A value of 3.5–5 monolayers of adsorbed species was obtained.

The temperature, shape, and relative intensity of the desorption peaks were not changed by repeated adsorption–TPD cycles, or by exposing Ni(A) to HCOOH ($\nu^s = 0.2\ s^{-1}$) at 473 K for 0.5 h. In the latter case, HCOOH decomposed catalytically with S equal to 4.5. After the catalytic reaction, the reactor was flushed with He at 473 K for 600 s, and heated ($\beta = 0.17\ K\ s^{-1}$) to 723 K. Only CO desorbed. It desorbed around 500 K, as in TPD of HCOOH preadsorbed on Ni(A).

Reduction of Ni powders in H_2 after one HCOOH adsorption–TPD cycle led to formation of CH_4 and H_2O. The consumption of H_2 was $1.0 \times 10^{14}\ cm^{-2}$, corresponding to 0.06 monolayers of oxygen atoms, or 0.03 monolayers of carbon atoms at the surface. The reduction occurred at higher temperature than the reduction of passivated Ni powders (Fig. 2). Apparently, the first peak involved reduction of a surface oxide ($\theta_0 = 0.01$) resulting from carrier gas impurities or from dissociated CO. The temperature of the other peak was similar to that reported for hydrogenation of molecularly adsorbed CO on Ni/Al_2O_3 (*23*). The area under this peak corresponded to 0.02 monolayers of adsorbed CO.

Isothermal Decomposition of Ni Formate

The decomposition of $Ni(OOCH)_2$ was autocatalytic. Conversion-time curves (α vs t) were sigmoidal, typical of bulk decomposition reactions involving nucleation and growth of a new phase. The data are described by either the equation of Avrami–Erofeev (*24, 25*),

$$\ln(1 - \alpha) = (kt)^2, \qquad (1)$$

or the equation of Prout–Tompkins (*26*),

$$\ln(\alpha/(1 - \alpha) = k^1 t + c \qquad (2)$$

(Fig. 3), where k, k^1, and c are constants. The activation energy E obtained from values of k and k^1 between 462 and 504 K is 94 kJ mol^{-1} (Table 2).

The selectivity S for decomposition was 3.5–5.0. It was independent of temperature, but increased slightly with conversion (Fig. 4, Table 2). Therefore, it was also independent of the concentration of products in the carrier gas, since the latter varied by a factor of 30 in the experimental temperature range. Therefore, CO and CO_2 are primary decomposition products which do not undergo secondary reactions as they are removed from the reaction zone. X-Ray diffraction of the passivated decomposition residue showed only metallic Ni.

TPD of Ni(OOCH)$_2$

The selectivity S of decomposition was 3.3–3.6. It was independent of temperature and conversion except at very low or high conversion, suggesting nearly coincident evolution of CO_2 and CO (Fig. 5). Evolution of H_2 occurred at the same temperature, namely, 475 K. The sharp peaks were typical of autocatalytic reactions (*10*).

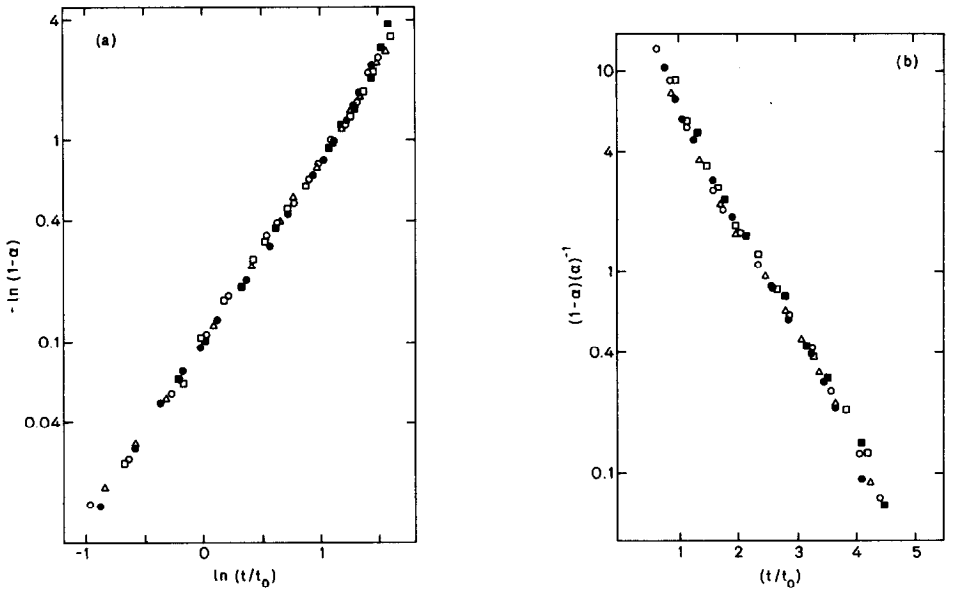

FIG. 3. Isothermal decomposition of bulk nickel formate. Decomposition rate expression. (a) Avrami–Erofeev equation (*24, 25*) $\ln(1-\alpha) = -(kt_0)^2(t/t_0)^2$ (t_0 = time required to decompose 10% of initial amount of formate). (b) Prout–Tompkins equation (*26*) $\ln(\alpha/1-\alpha) = kt_0(t/t_0) + C$; temperature (K): △, 462; ●, 469.5; ○, 479; □, 490; ■, 504.5.

The peak temperature (T_p) decreased from 500 to 465 K as the He contact frequency increased from 0.014 to 0.39 s^{-1}. This may result from the finite carrier gas residence time (*27, 28*), or from inhibition of the decomposition rate by the products. However, T_p was independent of dilution of formate by ground quartz; moreover, the ratio of carrier residence time to $\Delta T_{1/2}/\beta$ was 10^{-3}–10^{-4}, where $\Delta T_{1/2}$ denotes peak width at half maximum. Therefore, the finite carrier gas residence time should not affect T_p (*27, 28*). In addition, T_p for all products (CO_2, CO, H_2) changes identically with varying He contact frequency, even though their readsorption probability is undoubtedly different. Inhibition of formate decomposition rate by decomposition prod-

TABLE 2

Isothermal Decomposition of Bulk $Ni(OOCH)_2$

T (K)	t_0 (h)[a]	S[b]
504.5	0.062	3.6
490	0.125	3.9
479	0.20	3.9
469.5	0.31	3.9
462	0.47	3.9

[a] Time required to decompose 0.1 of the initial amount of formate.

[b] Ratio of CO_2 to CO in the decomposition products at 0.5 formate conversion.

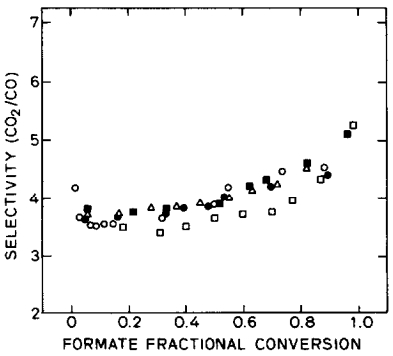

FIG. 4. Isothermal decomposition of bulk nickel formate. Composition of decomposition products (ν^b_{He} = 0.01 s^{-1}); temperature (K): ■, 462; ○, 469.5; ●, 479; △, 490; □, 504.5.

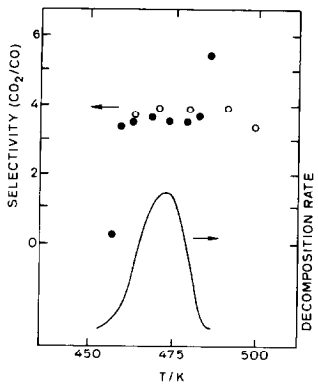

FIG. 5. TPD of bulk Ni formate. Decomposition products. ●, TPD (β = 0.04 K s^{-1}, ν^b_{He} = 0.2 s^{-1}); ○, isothermal decomposition, 0.5 fractional formate conversion.

ucts seems responsible for the increase in T_p with decreasing contact frequency.

DISCUSSION

Formate adsorbed on a fully covered surface was proposed as the reactive intermediate in the zero-order catalytic decomposition of HCOOH on Ni (*18, 31–34*). Formate also forms on Ni during HCOOH adsorption at room temperature. This agrees with infrared spectra obtained after HCOOH adsorption and during decomposition, with the decomposition product stoichiometry, with the evolution of H_2 during HCOOH adsorption, and with the selectivity S of decomposition, which resembles that of bulk $Ni(OOCH)_2$ (*18, 31–39*).

Previous data obtained by Madix and coworkers on TPD of HCOOH preadsorbed at low coverage on Ni (*1–3, 7*) and adlayer-covered Ni (*8, 15–17*) single crystals are shown in Table 3. As in the present study, CO_2 and H_2 evolved simultaneously at lower temperature than CO. However, S was near unity on Ni, and only greater than unity on C- or O-covered Ni. On Ni, the product composition corresponds to 0.2 monolayers of adsorbed formic anhydride, HCOOOCH. Its formation was said to require 4 adjacent Ni surface atoms. Formic anhydride molecules form surface islands and decompose autocatalytically due to attractive intermolecular forces which are very sensitive to surface orientation and structure.

In the present study, the surface density of adsorbed species is greater than that used by the Madix group, because of the much greater HCOOH exposures used, and the stoichiometry and decomposition selectivity of adsorbed species is different (4.0–5.5) from that in single crystal studies (*1–3, 7, 8, 15–17*). Apparently, the differences arise from an ensemble effect (*40*), inhibiting the formation of anhydride species on fully covered surfaces. Instead, surface formate species are formed, precluding subsequent anhydride formation as surface coverage decreases during TPD experiments. As previously proposed, adsorbed species requiring the least number of adjacent surface metal atoms are favored on fully covered surfaces. In other words, *structure-insensitive paths seem to be preferred on fully covered surfaces.*

The similar selectivity S obtained for bulk $Ni(OOCH)_2$ decomposition, TPD of HCOOH preadsorbed on Ni powder at high coverage, and catalytic HCOOH decomposition on Ni powder, Ni/SiO_2, and Ni/Al_2O_3 (Fig. 6) suggests a common formate species in all processes. It also suggests that sur-

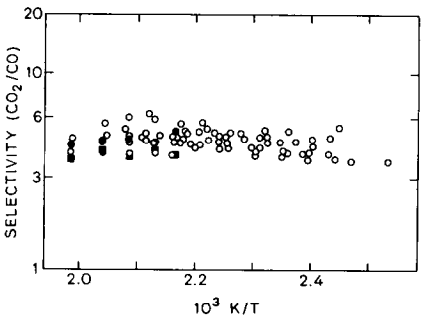

FIG. 6. Selectivity of the catalytic and temperature-programmed decomposition of HCOOH on Ni, and decomposition of bulk $Ni(OOCH)_2$. ■, Bulk Ni formate (0.5 fractional conversion); ●, bulk Ni formate (0.9 fractional conversion); ○, catalytic HCOOH decomposition on Ni powder, Ni/SiO_2 and Ni/Al_2O_3 (*18*).

face and subsurface formate decompose with similar selectivity. Two other explanations for the HCOOH TPD selectivity on Ni were ruled out. First, as in previous work (*8, 15–17*), surface formate may decompose exclusively to CO_2 and H_2, while subsurface layers decompose with selectivity characteristic of bulk $Ni(OOCH)_2$. However, 3–6 monolayers of formate on Ni(A) decomposed with identical selectivity. Second, formate only dehydrogenates, CO arising from CO_2 readsorption and decomposition. However, CO is a primary product in both catalytic HCOOH (*18*) and bulk formate decomposition, and CO_2 did not adsorb more than 0.04 of a monolayer on Ni powder at room temperature. Even at higher temperature, during TPD, CO_2 and H_2 desorb simultaneously, suggesting no binding site for either on these Ni samples. CO_2 readsorption and reaction to CO would lead to large surface oxygen coverages after TPD, since no surface hydrogen remains. Surface coverages of oxygen after TPD were about 0.01 monolayers.

Comparison of catalytic and TPD rates also suggests a common formate intermediate. Overlap among peaks prevents the calculation of rate constants from the peak shape (*29*) for HCOOH TPD on Ni powder. A preexponential factor A of 10^{13} s^{-1} was assumed and the activation energy E was calculated from the peak temperature using

$$E/RT_p^2 = (A/\beta)\exp[-E/RT_p]. \quad (3)$$

The isokinetic temperatures (T_0) calculated from these data and from catalytic rate data are compared in Table 3. In this case, T_0 is defined as the temperature required for a given value of the decomposition rate constant. It was shown (*30*) that T_0 depends mainly on the catalytic turnover rate and the TPD peak temperature, and not on the values of A and E chosen to describe them. The catalytic dehydrogenation T_0 agrees with those calculated for the (α) and (β) CO_2 and H_2 peaks (Table 3). However, dehydration T_0 values differ from those for the CO evolution peak because the latter is desorption- rather than decomposition-limited in TPD experiments. Catalytic isokinetic temperatures reflect the kinetics of the rate limiting step, which in this case is the decomposition of surface formate; CO desorption steps are in equilibrium (*18*).

TABLE 3a

Rate Constants Calculated from TPD of HCOOH Preadsorbed on Ni: This Study

	Desorption product	T_p[a] (K)	E[b] (kJ mol^{-1})	Isokinetic temperature[c] (K)	S[d]
Ni	$H_2(\alpha)$	371	105	397	
	$H_2(\gamma)$	441	126	475	5.2
	$CO_2(\alpha)$	378	107	405	±
	$CO_2(\gamma)$	443	127	477	0.5
	$CO(\alpha)$	480	137	518	
	$CO(\beta)$	505	145	546	
Ni(A)	$H_2(\alpha)$	356	102	382	
	$H_2(\beta)$	400	114	430	
	$H_2(\gamma)$	450	129	485	4.0
	$CO_2(\alpha)$	359	102	384	±
	$CO_2(\beta)$	403	115	433	0.5
	$CO_2(\gamma)$	446	127	480	
	$CO(\alpha)$	468	134	505	
	$CO(\beta)$	516	148	559	

[a] $\beta = 0.18$ K s^{-1}.

[b] Assumed first-order reaction in adsorbed species with preexponential factor equal to 10^{13} s^{-1}.

[c] $N = 0.16$ s^{-1}, assuming 1.5×10^{15} cm^{-2} density of adsorbed intermediates.

[d] Ratio of CO_2 to CO in decomposition products.

Differences in the relative intensities of various desorption peaks between the two Ni catalysts may reflect different concentrations of surface defects or crystallographic planes which give rise to the multiple desorption peaks. However, the peak temperatures, and therefore the desorption and decomposition energies, are similar on the two Ni catalysts.

Values of selectivity for catalytic HCOOH decomposition and bulk Ni $(OOCH)_2$ decomposition are also similar. Bulk $Ni(OOCH)_2$ decomposes with S equal to 3.5–5.0; S does not depend on conversion, temperature, or product concentration in the carrier gas. Therefore, CO_2, CO,

TABLE 3b

Rate Constants Calculated from TPD of HCOOH Preadsorbed on Ni: Literature Data

Sample	Decomposition product	Ref.	A (s^{-1})	E (kJ mol^{-1})	Isokinetic temperature[b] (K)	S[c]	σ[d] (10^{15} cm^{-2})
TPD							
Ni(110)	CO_2, H_2	1–3, 11	6×10^{15}	118[a]	370	1.0	0.18
	CO	1–3, 11	1×10^{15}	111	365	—	0.18
Ni(110)	CO_2, H_2	11	6×10^{15}	112.5[a]	353	—	0.2
	CO	11	1×10^{15}	109	358	—	—
Ni(110)	CO_2, $H_2(\beta_1)$	6	4×10^{12}	106.5	413	3–10	0.15
$(2 \times 1)C$	CO_2, $H_2(\beta_2)$	6	1×10^{11}	104.5	460	—	0.15
Ni(100) $p(2 \times 2)C$	CO_2, H_2	12	8×10^{14}	118.5	392	∞	0.4
Ni(110)	CO_2, H_2	7	1.6×10^{12}	84.5	340	3	0.16
$(2 \times 1)O$	CO	7	4×10^{12}	106	411	—	0.05
Catalytic decomposition							
Ni	CO_2	16	4×10^{11}–1×10^{13}	100–111	418–420	3.5–6	—
powder	CO	16	1×10^{10}–2×10^{12}	93–111	438–447		—
Silica-supported Ni	CO_2	16	5×10^{11}–2×10^{12}	105–107	425–434	4.0–5.5	—
	CO	16	6×10^{10}–2×10^{11}	100–105	447–461		—

[a] At saturation coverage.
[b] $N = 0.16$ s^{-1}, assuming 1.5×10^{15} cm^{-2} surface density of intermediates.
[c] Ratio of CO_2 to CO in decomposition products.
[d] Saturation coverage of adsorbed formic anhydride or formate species.

and H_2 are primary decomposition products. S is not affected by secondary reactions, and it is solely determined by the relative strengths of hydrogen and oxygen surface bonds in the activated formate complex. Selectivity is similar to some values previously reported for $Ni(OOCH)_2$ decomposition (*20, 41, 42*), but disagrees with others (*43, 46*). It is similar to values reported for catalytic HCOOH decomposition, and TPD of HCOOH preadsorbed on Ni (Fig. 6). The activation energy for Ni $(OOCH)_2$ decomposition (94 kJ mol^{-1}) agrees with values of 96 kJ mol^{-1} (*20*) and 88 kJ mol^{-1} (*44, 45*) previously reported. It also resembles that of the catalytic (93–111 kJ mol^{-1}) (*18*) and of the temperature-programmed (109–129 kJ mol^{-1}) decomposition of HCOOH on Ni. The bulk Ni $(OOCH)_2$ decomposition rate, but not S, depends on the concentration of products. A similar effect was reported for the catalytic reaction on Ni and Ni/SiO_2.

In conclusion, on both Cu (*22*) and Ni, HCOOH preadsorbed at a coverage higher than two-tenths of a monolayer seems to decompose through a formate intermediate with a selectivity similar to that for catalytic HCOOH decomposition on the respective metal and for the decomposition of the respective bulk formate. This suggests that catalytic HCOOH decomposition occurs through a formate intermediate. No evidence was found for a formate anhydride intermediate, previously proposed for TPD of HCOOH preadsorbed at low coverage on Ni single crystals (*1–7*). Again, it appears that structure insensitive paths seem to be favored on fully covered surfaces. This may explain discrepancies between results obtained at low pressure and at high pressure.

REFERENCES

1. McCarty, J., Falconer, J. L., and Madix, R. J., *J. Catal.* **30,** 235 (1973).
2. McCarty, J., Falconer, J. L., and Madix, R. J., *J. Catal.* **31,** 316 (1973).
3. Falconer, J. L., and Madix, R. J., *Surface Sci.* **46,** 473 (1974).
4. Falconer, J. L., and Madix, R. J., *Surface Sci.* **48,** 262 (1975).
5. Falconer, J. L., and Madix, R. J., *J. Catal.* **48,** 262 (1977).
6. Falconer, J. L., and Madix, R. J., *J. Catal.* **51,** 47 (1978).
7. Benziger, J. B., and Madix, R. J., *Surface Sci.* **79,** 394 (1979).
8. Ying, D. H. S., Ph.D. Dissertation, Stanford University, 1978.
9. Ying, D. H. S., and Madix, R. J., *J. Catal.* **61,** 48 (1980).
10. Madix, R. J., *Catal. Rev.* **15,** 293 (1977).
11. Barteau, M. A., Bowker, M., and Madix, R. J., *J. Catal.* **67,** 118 (1981).
12. Benziger, J. B., Ph.D. Dissertation, Stanford University, 1979.
13. Abbas, N., Ph.D. Dissertation, Stanford University, 1981.
14. Benziger, J. B., Ko, E. I., and Madix, R. J., *J. Catal.* **58,** 149 (1979).
15. McCarty, J., and Madix, R. J., *J. Catal.* **38,** 402 (1975).
16. McCarty, J., and Madix, R. J., *Surface Sci.* **54,** 210 (1976).
17. Johnson, S. W., and Madix, R. J., *Surface Sci.* **66,** 189 (1977).
18. Iglesia, E., and Boudart, M., *J. Catal.* **81,** 224 (1983).
19. Iglesia, E., and Boudart, M., *J. Catal.* **81,** 204 (1983).
20. Bircumshaw, L. L., and Edwards, J., *J. Chem. Soc.* 1800 (1950).
21. Martin, R. L., and Waterman, H., *J. Chem. Soc.* 1359 (1959).
22. Iglesia, E., and Boudart, M., *J. Catal.* **81,** 214 (1983).
23. Galwey, A. K., Jamieson, D. M., and Brown, M. E., *J. Phys. Chem.* **78,** 2664 (1974).
24. Avrami, M., *J. Chem. Phys.* **1,** 1103 (1939).
25. Erofeev, B. V., *Dokl. Akad. Sci. USSR* **52,** 511 (1946).
26. Prout, E. G., and Tompkins, F. C., *Trans. Faraday Soc.* **40,** 488 (1944).
27. Taylor, J. L., and Weinberg, W. H., *Surface Sci.* **78,** L508 (1978).
28. Chan, C. M., Aris, R. A., and Weinberg, W. H., *Appl. Surface Sci.* **1,** 377 (1978).
29. Edwards, D., *Surface Sci.* **54,** 1 (1976).
30. Iglesia, E., Ph.D. Dissertation, Stanford University, 1981.
31. Fahrenfort, J., van Reijen, L. L., and Sachtler, W. M. H., *in* "The Mechanism of Heterogeneous Catalysis" (de Boer, J. H., Ed.), p. 23. Elsevier, Amsterdam, 1960.
32. Fahrenfort, J., van Reijen, L. L., and Sachtler, W. M. H., *Z. Elektrochem.* **64,** 216 (1960).
33. Fukuda, K., Nagishima, S., Noto, Y., Onishi, T., and Tamaru, K., *Trans. Faraday Soc.* **64,** 522 (1968).
34. Tamaru, K., *Trans. Faraday Soc.* **55,** 824 (1959).
35. Hirota, K., Kuwata, K., and Nakai, Y., *Bull. Chem. Soc. (Japan)* **31,** 861 (1958).
36. Hirota, K., Otaki, T., and Asai, S., *Z. Phys. Chem. (N.F.)* **21,** 438 (1959).
37. Hirota, K., Kuwata, K., Otaki, T., and Asai, S., *in* "Actes Deuxieme Congres International de Catalyse," p. 809. Technip, Paris, 1960.
38. Fahrenfort, J., and Hazebroek, H. F., *Z. Phys. Chem. (N.F.)* **20,** 105 (1959).
39. Eischens, R. E., and Pliskin, W. A., *in* "Actes Deuxieme Congres International de Catalyse," p. 789. Technip, Paris, 1960.
40. Sachtler, W. M. H., *Vide* **164,** 67 (1973).
41. Balandin, A. A., Grigoryan, E. S., and Yanisheva, Z. S., *J. Gen. Chem. USSR* **10,** 1031 (1940).
42. Krogmann, K., *Z. Anorg. Chem.* **307,** 16 (1961).
43. Carrion, J., Criado, J. M., Herrera, D. J., and Torres, C., *in* "Proceedings of the 8th International Symposium on the Reactivity of Solids" (N. G. Vannerberg and C. Helgesson, Eds.), p. 267. Plenum, New York, 1977.
44. Criado, J. M., Gonzalez, F., and Trillo, J. M., *Rev. Chim. Minerale* **7,** 1041 (1970).
45. Criado, J. M., Gonzalez, F., and Morales, J., *Thermochim. Acta* **12,** 337 (1975).
46. Fox, P. G., Ehretsmann, J., and Brown, C. E., *J. Catal.* **20,** 67 (1971).